The Astrophysical Journal, 821:36 (10pp), 2016 April 10 doi:10.3847/0004-637X/821/1/36

MAGNETAR-DRIVEN SHOCK BREAKOUT AND DOUBLE-PEAKED SUPERNOVA LIGHT CURVES

Daniel Kasen[1,2], Brian D. Metzger[3], and Lars Bildsten[4,5]
[1] Nuclear Science Division, Lawrence Berkeley National Laboratory, Berkeley, CA 94720, USA
[2] Departments of Physics and Astronomy, University of California, Berkeley, CA 94720, USA
[3] Columbia Astrophysics Laboratory, Columbia University, New York, NY 10027, USA
[4] Kavli Institute for Theoretical Physics, University of California, Santa Barbara, CA 93106, USA
[5] Department of Physics, University of California, Santa Barbara, CA 93106, USA
Received 2015 July 13; accepted 2015 December 11; published 2016 April 6

ABSTRACT

The light curves of some luminous supernovae are suspected to be powered by the spindown energy of a rapidly rotating magnetar. Here we describe a possible signature of the central engine: a burst of shock breakout emission occurring several days after the supernova explosion. The energy input from the magnetar inflates a high-pressure bubble that drives a shock through the pre-exploded supernova ejecta. If the magnetar is powerful enough, that shock will near the ejecta surface and become radiative. At the time of shock breakout, the ejecta will have expanded to a large radius ($\sim 10^{14}$ cm) so that the radiation released is at optical/ultraviolet wavelengths ($T_{\rm eff} \approx 20{,}000$ K) and lasts for several days. The luminosity and timescale of this magnetar-driven shock breakout are similar to the first peak observed recently in the double-peaked light curve of SN-LSQ14BDQ. However, for a large region of model parameter space, the breakout emission is predicted to be dimmer than the diffusive luminosity from direct magnetar heating. A distinct double-peaked light curve may therefore only be conspicuous if thermal heating from the magnetar is suppressed at early times. We describe how such a delay in heating may naturally result from inefficient dissipation and thermalization of the pulsar wind magnetic energy. Without such suppression, the breakout may only be noticeable as a small bump or kink in the early luminosity or color evolution, or as a small but abrupt rise in the photospheric velocity. A similar breakout signature may accompany other central engines in supernovae, such as a black hole accreting fallback material.

Key words: shock waves – stars: magnetars – stars: neutron – supernovae: general

1. INTRODUCTION

Optical surveys are finding a growing number of brilliant, though rare, explosive transients, some 10−100 times brighter than ordinary core-collapse supernovae (SNe; Ofek et al. 2007; Quimby et al. 2007; Smith et al. 2007; Barbary et al. 2009; Pastorello et al. 2010; Chomiuk et al. 2011; Quimby et al. 2011; Gal-Yam 2012; Howell et al. 2013; Inserra et al. 2013; Nicholl et al. 2014; Papadopoulos et al. 2015). The mechanism generating these enormous luminosities is unclear; the energy sources that power ordinary SN light curves—the diffusion of shock deposited thermal energy, or heating by radioactive ^{56}Ni—appear incapable of reproducing the observed rise time and peak brightness of many of the superluminous SNe (SLSNe).

Two classes of models are frequently invoked to explain the light curves of SLSNe. The first involves interaction of the SN ejecta with an extended circumstellar medium (CSM). If interaction occurs at a location where the ejecta is translucent (radii $\sim 10^{15}$ cm), the thermalized kinetic energy can be radiated efficiently (Smith & McCray 2007; Woosley et al. 2007; Chevalier & Irwin 2011; Moriya et al. 2011). In the second class of models, the ejecta from a seemingly ordinary SN explosion is continuously reheated via energy injection from a long-lived central engine, either a rapidly rotating, highly magnetized neutron star (a millisecond magnetar; Kasen & Bildsten 2010; Woosley 2010) or an accreting black hole (Dexter & Kasen 2013).

Observations provide some evidence for both ideas. In the class of Type II SLSNe, narrow ($\sim$10–100 km s^{-1}) hydrogen Balmer lines are often seen in emission, a signature of interaction with a slow-moving CSM. In the Type I SLSNe, on the other hand, no spectroscopic indications of interaction are apparent and the line features only indicate rapidly moving ($\sim$10,000–15,000 km s^{-1}) material. The magnetar-powered model of SLSNe has been successful in fitting the light curves, colors, photospheric velocity evolution, and gross spectral features of several Type I SLSNe (Dessart et al. 2012; Howell et al. 2013; Inserra et al. 2013; Nicholl et al. 2013). Late-time observations of some Type I SLSNe show emission continuing for hundreds of days after the explosion, which has been claimed to be indicative of persistent magnetar heating (Inserra et al. 2013).

Additional observational tests are needed to validate and discriminate models of SLSNe. Such an opportunity may have arisen with the well-sampled photometry of SN-LSQ14BDQ (Nicholl et al. 2015), a Type I SLSN with a double-peaked light curve. The luminosity of SN-LSQ14BDQ rose to an early maximum in $\approx$5 days; then, after a brief decline, the light curve rose again to an even brighter peak ($\approx 2 \times 10^{44}$ erg s^{-1}) by 50 days later. A similar double-peaked morphology had already been seen in the light curve of the SLSN SN 2006oz (Leloudas et al. 2012), although with poorer temporal sampling, and in SN 2005bf, an unusual SN Ib of more ordinary brightness (Anupama et al. 2005; Folatelli et al. 2006; Maeda et al. 2007).

Here we describe how a magnetar may produce a double-peaked light curve. The key insight is that a central engine heats the SN ejecta in two physically and spatially distinct ways. A thermalized pulsar wind heats the ejecta directly at its base, powering a luminosity that diffuses out on timescales of weeks or months. At the same time, the pulsar wind dynamically affects the ejecta, inflating a high-pressure bubble that drives shock heating at larger radii. If the magnetar is

powerful enough, that shock will near the ejecta surface and become radiative, producing an early burst of emission.

The situation resembles, in some ways, shock breakout from a stellar explosion (Klein & Chevalier 1978; Matzner & McKee 1999), with a few key differences. First, a magnetar-driven shock propagates through a moving medium; the shock will be weaker, and when it does emerge, the ejecta surface will have expanded by several orders of magnitude in radius. The resulting emission will last longer and be at longer wavelengths (optical/UV) than the brief X-ray burst that accompanies ordinary SN shock breakout. Second, the shock does not necessarily die once it becomes radiative; as long as the magnetar continues to inject energy, the shell can be driven faster than free expansion and may release energy at its outer edge.

The integrated heating from a magnetar-driven shock amounts to only a few percent of the total pulsar wind energetics. However, shock heating occurs exterior to the bulk of the ejecta and so can be radiated $\lesssim$1 week after explosion, before most of the centrally thermalized energy has had time to diffuse out. Under certain circumstances, the two heating mechanisms may produce two distinct emission maxima. We develop below an analytic description of "magnetar-driven shock breakout" and present toy light-curve calculations that suggest that this effect provides an appealing explanation for double-peaked SN light curves and a means to constrain the magnetar model of SLSNe.

2. DYNAMICS OF MAGNETAR-DRIVEN SHOCKS

Consider a pulsar with spin period P and magnetic field B. The total spin energy is

$$E_{\rm m} \approx 2 \times 10^{52} P_{\rm ms}^{-2} \ {\rm erg}, \tag{1}$$

where $P_{\rm ms} = P/1$ ms and we adopt a neutron star moment of inertia of $I = 10^{45}$ g cm^2. The rate at which energy is input from the pulsar is, in the case of vacuum magnetic dipole spindown,

$$L_{\rm m} = \frac{E_{\rm m}/t_{\rm m}}{(1 + t/t_{\rm m})^2}, \tag{2}$$

where the spindown timescale is

$$t_{\rm m} \approx 5 B_{14}^{-2} P_{\rm ms}^2 \ {\rm days}, \tag{3}$$

where $B_{14} = B/10^{14}$ G and we assume, as in Kasen & Bildsten (2010), that the angle between the rotation axis and magnetic dipole is $\alpha = 45°$. If the spindown energy is thermalized in the ejecta, it may power an SN light curve (Bodenheimer & Ostriker 1974; Gaffet 1977; Maeda et al. 2007; Kasen & Bildsten 2010; Woosley 2010). The dynamical effect of the energy injection, however, is independent of whether it thermalizes or not; in either case the energy behaves as a $\gamma = 4/3$ gas.

We will assume that the SN ejecta of mass $M_{\rm sn}$ is spherically symmetric and has a broken power-law density profile, with a shallow profile in the inner region and a steep one in the outer regions (Chevalier & Soker 1989). The transition occurs at a velocity coordinate

$$v_{\rm t} = \zeta_v (E_{\rm sn}/M_{\rm sn})^{1/2}. \tag{4}$$

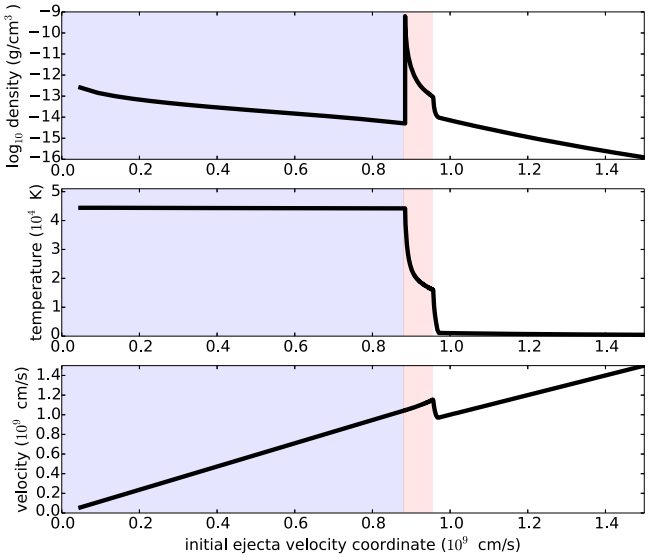

Figure 1. 1D hydrodynamical calculation of the dynamical effect of a magnetar on the SN ejecta. The ejecta had $M_{\rm sn} = 5\,M_\odot$, and initially $E_{\rm sn} = 10^{51}$ erg and a broken power-law density profile (Equation (5)). Energy injection from a magnetar with $E_{\rm m} = 5 \times 10^{51}$ erg and $t_{\rm m} = 5$ days was input according to Equation (2) in the inner few zones of the ejecta. The snapshot shown is at a time $t = 15$ days. The blue shading highlights the low-density, high-temperature magnetar bubble. The red shading shows the region heated by the magnetar-driven shock. Radiation diffusion has not been included in this calculation.

In the inner ejecta ($v < v_{\rm t}$) the density at a position r and time t is

$$\rho(r, t) = \zeta_\rho \frac{M_{\rm sn}}{v_{\rm t}^3 t^3} \left(\frac{r}{v_{\rm t} t}\right)^{-\delta}. \tag{5}$$

The density profile in the outer ejecta ($v > v_{\rm t}$) has the same form but a different exponent, $\rho \propto r^{-n}$. The coefficients are given by

$$\zeta_\rho = \frac{(n-3)(3-\delta)}{4\pi(n-\delta)}, \tag{6}$$

$$\zeta_v = \left[\frac{2(5-\delta)(n-5)}{(n-3)(3-\delta)}\right]^{1/2}. \tag{7}$$

Typical values for core-collapse SNe are $\delta = 1$, $n = 10$ (Chevalier & Soker 1989), which we adopt as fiducial.

For $E_{\rm m} \gtrsim E_{\rm sn}$, the magnetar wind will significantly restructure the SN ejecta, as illustrated in the hydrodynamical calculation of Figure 1. The high pressure from central energy injection evacuates a cavity and sweeps ejecta into a thin shell. The shell moves faster than the local ejecta expansion velocity, and a radiation-dominated shock of relative velocity $\approx$2500 km s^{-1} forms. In a multidimensional calculation, Rayleigh–Taylor instabilities would break apart the shell and smear out the density peak (e.g., Blondin et al. 2001), but the global structure would be qualitatively similar. In addition, at late times, radiation diffusion from the inner hot bubble will smear out the temperature discontinuity at the shock front.

2.1. Time of Shock Emergence

The magnetar-driven shock will become radiative when the diffusion time to the ejecta surface, $t_{\rm diff} \sim \tau R/c$, becomes

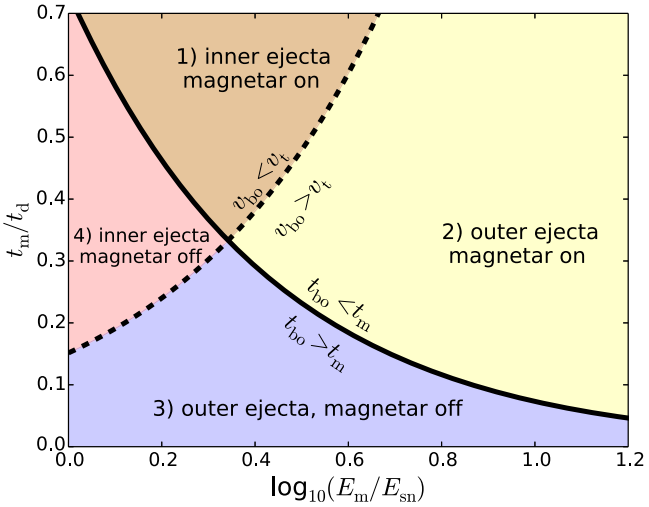

Figure 2. Different regimes of magnetar-driven shock emergence, illustrating whether the shock becomes radiative in the inner ejecta ($v_{bo} < v_t$) or outer ejecta ($v_{bo} > v_t$) and whether the magnetar is "on" ($t_{bo} < t_m$) or "off " ($t_{bo} > t_m$) at the time of emergence. The solid lines are determined from Equations (18) and (19) with $\alpha = 5/4$ and $n = 10$. Breakout emission can occur in all regions, but will be brightest in region 2, when the shock is strongest.

comparable to the elapsed time, $t \sim R/v$, or when the shock reaches an optical depth $\tau \sim c/v$. In the outer ejecta, the optical depth from the surface inward to velocity coordinate v is

$$\tau(v) = \frac{1}{(n-1)}\frac{c}{v_t}\frac{t_d^2}{t^2}\left(\frac{v}{v_t}\right)^{-n+1}, \quad (8)$$

where

$$t_d = \left[\frac{\zeta_\rho M_{sn}\kappa}{v_t c}\right]^{1/2} \approx 32\, M_{sn,5}^{3/4} E_{sn,51}^{-1/4}\kappa_{0.1}^{1/2}\ \text{days} \quad (9)$$

is the effective diffusion time in a homologous expanding medium (Arnett 1982). Here $M_{sn,5} = M_{sn}/5M_\odot$, $E_{sn,51} = E_{sn}/10^{51}$ erg, and $\kappa_{0.1} = \kappa/0.1\ \text{cm}^2\ \text{g}^{-1}$ is the scaled opacity. The shock then becomes radiative ($\tau = c/v$) when it reaches a radius

$$r_{bo} = v_t t\left[\frac{1}{\sqrt{n-1}}\frac{t_d}{t}\right]^{2/(n-2)}. \quad (10)$$

Equation (10) assumes that r_{bo}/t lies above the transition velocity coordinate v_t, which is true for $t < t_d/\sqrt{n-1} \approx 10$ days.

To determine the time when the shock reaches the breakout radius r_{bo}, we make the assumption that mass is swept up into a geometrically thin shell (Ostriker & Gunn 1971; Chevalier 1984; Chevalier & Fransson 1992). The momentum and energy equations describing the shell dynamics are

$$M_s\frac{dv_s}{dt} = 4\pi r_s^2[p_b - \rho(v_s - v_{ej})^2], \quad (11)$$

$$\frac{d(4\pi r_s^3 p_b)}{dt} = -4\pi p_b r^2\frac{dr_s}{dt} + L_m(t) - L_{sn}(t), \quad (12)$$

where M_s, r_s, and v_s are the mass, radius, and velocity of the shell, respectively, $v_{ej} = r_s/t$ is the ejecta velocity at radius r_s, ρ is the preshock ejecta density ahead of the shell, and p_b is the pressure in the magnetar-inflated bubble. The L_{sn} term represents the rate at which thermalized magnetar wind energy radiatively diffuses out of the bubble.

Assuming that the magnetar injects energy at a nearly constant rate, $L_m = E_m/t_m$, and that diffusion losses can be ignored ($L_{sn} \approx 0$, appropriate for $t \ll t_d$), the dynamical equations have self-similar power-law solutions for r_s and p_b (Chevalier & Fransson 1992),

$$r_s(t) = v_t t_{tr}^{1-\alpha} t^\alpha, \quad (13)$$

where $\alpha = (6-\delta)/(5-\delta)$ and

$$t_{tr} = \zeta_{tr}\left(\frac{E_{sn}}{E_m}\right)t_m \quad (14)$$

is the time it takes the shell to propagate through the inner ejecta and reach the transition velocity v_t. The coefficient is

$$\zeta_{tr} = \left[\frac{2(n-5)(9-2\delta)(11-2\delta)}{(5-\delta)^2(n-\delta)(3-\delta)}\right]. \quad (15)$$

For $n = 10$, $\delta = 1$, we have $\alpha = 5/4$ and $\zeta_{tr} = 2.2$. The expression for t_{tr} has been previously derived in Chevalier (2005).

This self-similar power-law solution only holds for times $t < t_{tr}$ when the shell remains in the inner ejecta. At later times, the shell moves into the steep outer ejecta and accelerates. The shock front will begin to move ahead of the shell, but the thin-shell approximation appears to remain reasonably valid (see Figure 1). The limiting behavior can be understood by noting that, at large radius, nearly all of the mass is swept into the shell, $M_s \to M_{sn}$. Given the low densities in the outer ejecta, the ram pressure term $\rho(v_s - v_{ej})^2$ can be neglected relative to the bubble pressure, and the dynamical equations give asymptotically a power law (Equation (13)) with $\alpha = 3/2$.

Although the break in the density profile complicates the dynamics, the shell radius can be reasonably approximated by $r_s \propto t^\alpha$ where the exponent is in the range $\alpha \approx 1.2$–1.5. If we assume that the shock becomes radiative in (or near) the outer ejecta, the time of shock breakout is found by setting r_s equal to the breakout radius, r_{bo} (Equation (10)), giving

$$t_{bo} \approx \left[\frac{\zeta_{tr}^{1-\beta}}{(n-1)^{\beta/2}}\right] t_d^\beta t_m^{1-\beta}(E_{sn}/E_m)^{1-\beta}, \quad (16)$$

where

$$\beta = \frac{2}{(\alpha-1)(n-2)+2}. \quad (17)$$

The shock breakout time, t_{bo}, is a weighted geometric mean of t_d and t_m, where the appropriate value of β depends on whether the shell has spent most of its time in the inner or outer regions of ejecta, i.e., whether t_{bo} is much greater than or less than t_{tr}. For $t_{bo} \lesssim t_{tr}$, the self-similar value $\alpha \approx 5/4$ applies, and $\beta = 1/2$ (for $n = 10$). For $t_{bo} \gg t_{tr}$, the asympotic value $\alpha = 3/2$ is more accurate and $\beta = 1/3$. The distinguishing condition is

$$t_{bo} \gtrsim t_{tr} \ \text{ if } \ E_m \gtrsim 6.6E_{sn}\frac{t_m}{t_d}. \quad (18)$$

To further complicate the dynamics, at times $t > t_m$, the energy input from the magnetar "shuts off," i.e., L_m drops

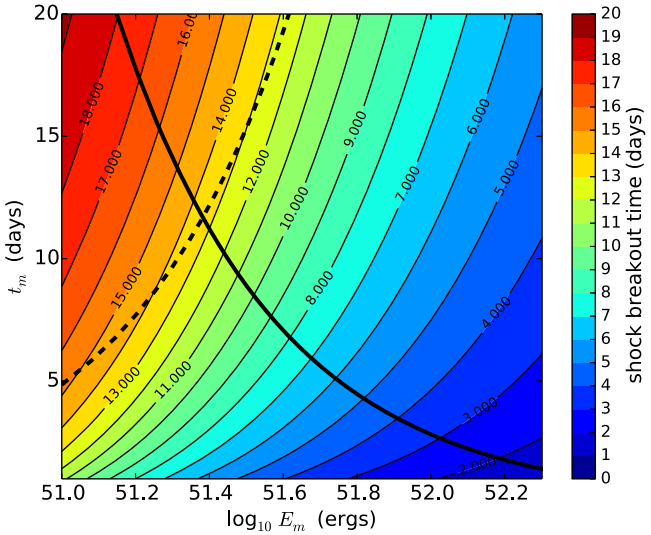

Figure 3. Numerical calculation of the shock breakout time, $t_{\rm bo}$, for various values of $E_{\rm m}$ and $t_{\rm m}$ and standard ejecta parameters: $M_{\rm sn} = 5\,M_\odot$, $E_{\rm sn} = 10^{51}$ erg, $\delta = 1$, $n = 10$, $\kappa = 0.1$ g cm^2, which imply a diffusion time $t_{\rm d} = 32$ days. The magnetar energy injection rate was taken from Equation (2). The solid line shows the estimated $t_{\rm bo} = t_{\rm m}$ contour from Equation (19); the dashed line shows the estimated $v_{\rm bo} = v_{\rm t}$ contour from Equation (18).

toward zero. Following this, the bubble pressure decreases nearly adiabatically and the shell radius approaches free expansion, $r_{\rm s} \propto t$. A shock breakout can still occur, but the emission will be less luminous because the shock speed declines for $t > t_{\rm m}$. The brightest shock breakouts then occur when the shock becomes radiative before the magnetar shuts off, which requires a magnetar energy

$$t_{\rm bo} < t_{\rm m} \;\; \text{if} \;\; E_{\rm m} \gtrsim 0.7 E_{\rm sn} \left(\frac{t_{\rm d}}{t_{\rm m}}\right)^{\beta/(1-\beta)}. \qquad (19)$$

The two conditions (Equations (18) and (19)) divide the $E_{\rm m}$–$t_{\rm m}$ parameter space of shock emergence into four regimes, illustrated in Figure 2. The partitioning is only suggestive, as real ejecta density profiles are more complex than a broken power law, and the magnetar energy deposition does not shut off sharply, but rather follows a smooth function of the form given by Equation (2). The most luminous breakouts occur when the shock is being continuously driven through the steep outer ejecta (region 2), which happens when the magnetar is energetic and/or long lasting. On the other extreme, for $E_{\rm m} \ll E_{\rm sn}$ or $t_{\rm m} \ll t_{\rm d}$ the shock will stall out before being revealed, and no prominent shock breakout signature is expected.

To better determine the time of shock emergence, we numerically integrated the dynamical equations (Equations (11) and (12)) to follow the shell location and find when it reached the $\tau = c/v$ surface. This calculation did not assume $L_{\rm sn} = 0$, but rather included approximate radiative loses via the method described in the Appendix. Figure 3 shows this calculation of $t_{\rm bo}$ for various values of $E_{\rm m}$ and $t_{\rm m}$ and standard ejecta parameters. When we carry out the numerical integration using $L_{\rm m}$ constant for $t < t_{\rm m}$ and zero afterward, the resulting $t_{\rm bo}$ agrees well with the analytic expression given by Equation (16). For the more realistic case of continuous energy injection (given by Equation (2)) the analytic result underestimates $t_{\rm bo}$ by about 20%. In this case, a better estimate is achieved by multiplying $t_{\rm m}$ in Equation (16) by a factor of $\approx$1.5

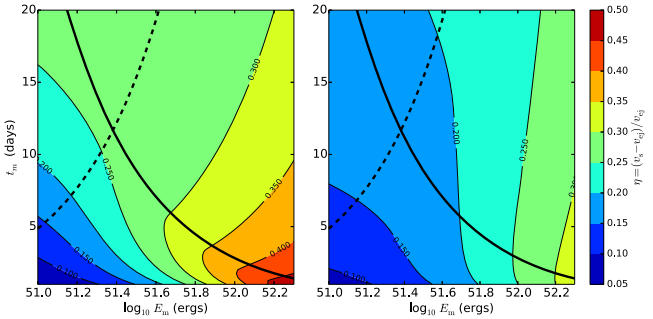

Figure 4. Numerical calculation of the shock strength parameter $\eta = (v_{\rm s} - v_{\rm ej})/v_{\rm ej}$ at the time of shock breakout for various values of $E_{\rm m}$ and $t_{\rm m}$ and standard ejecta parameters: $M_{\rm sn} = 5\,M_\odot$, $E_{\rm sn} = 10^{51}$ erg, $\delta = 1$, $n = 10$, $\kappa = 0.1$ cm^2 g^{-1}. The left panel assumes a constant magnetar energy injection rate $L_{\rm m} = E_{\rm m}/t_{\rm m}$ for $t < t_{\rm m}$ and $L_{\rm m} = 0$ afterward. The right panel uses the continuous injection rate of Equation (2). The solid line shows the estimated $t_{\rm bo} = t_{\rm m}$ contour from Equation (19); the dashed line shows the estimated $v_{\rm bo} = v_{\rm t}$ contour from Equation (18).

to account for the nonzero magnetar energy injection at later times.

2.2. Shock Heating

We next estimate the local heating from the magnetar-driven shock, which will set the luminosity of breakout when the shock emerges. The rate at which energy is dissipated at the shock is

$$\dot{\epsilon}_{\rm sh}(t) = 4\pi r_{\rm s}^2 \frac{\rho}{2}(v_{\rm s} - v_{\rm ej})^3 = 4\pi r_{\rm s}^2 \frac{\rho}{2} v_{\rm ej}^3 \eta^3, \qquad (20)$$

where in the second expression we have parameterized the shock velocity as

$$\eta(t) = \frac{v_{\rm s} - v_{\rm ej}}{v_{\rm ej}} = \frac{t}{r_{\rm s}}\left(\frac{dr_{\rm s}}{dt} - \frac{r_{\rm s}}{t}\right). \qquad (21)$$

The shock strength parameter η will play an important role in determining the radiated luminosity. If the shell radius obeys a power law, $r_{\rm s} \propto t^\alpha$, then $\eta = \alpha - 1$. In the inner ejecta, α approaches the self-similar value $\alpha = (6 - \delta)/(5 - \delta)$ and $\eta = 1/(5 - \delta)$, or $\eta = 1/4$ for $\delta = 1$. In other words, the shell moves 25% faster than the local ejecta velocity. For $t \gg t_{\rm tr}$, when the shock propagates deep into the steep outer ejecta and accelerates, $\alpha \to 3/2$ and $\eta \to 1/2$.

Using our numerical integration of the dynamical equations discussed in Section 2, we calculated the value of η at the time of shock emergence. The left panel of Figure 4 shows the numerical determination of η for the simple case where $L_{\rm m} = E_{\rm m}/t_{\rm m}$ is constant for $t < t_{\rm m}$ and then immediately drops to $L_{\rm m} = 0$. The behavior follows analytical expectations: in region 1 (shock emergence in the inner ejecta, magnetar on) $\eta = 0.25$; in region 2 (shock emergence in the outer ejecta, magnetar on) $\eta > 0.25$ and increases with increasing magnetar energy, approaching a maximum value $\eta = 0.5$. For region 3 (shock emergence in the outer ejecta, magnetar off) η declines as $t_{\rm m}$ decreases, illustrating the progressive weakening of the shock following magnetar shutoff.

The right panel of Figure 4 shows the behavior of η in a calculation using continuous magnetar energy injection given by Equation (2). Similar trends with $E_{\rm m}$ and $t_{\rm m}$ are seen, but the values of η are generally lower, as the magnetar energy

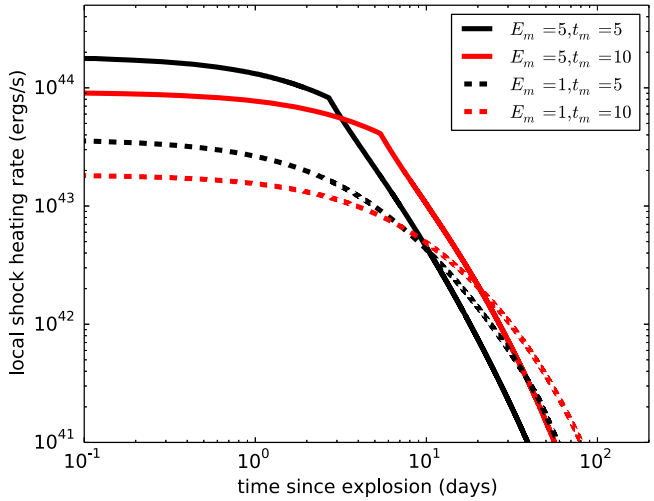

Figure 5. Calculation of the local shock heating rate (Equation (20)) over time for standard ejecta parameters $M_{\rm sn} = 5\,M_\odot$, $E_{\rm sn} = 10^{51}$ erg, $\delta = 1$, $n = 10$, and continuous magnetar energy injection given by Equation (2). The legend gives the value of the magnetar energy (in units of 10^{51} erg) and the spindown time (in days). A power-law break in the heating rate is seen when the shock enters the steep density profile of the outer ejecta. The luminosity of shock breakout is approximately the local heating rate at the time of breakout.

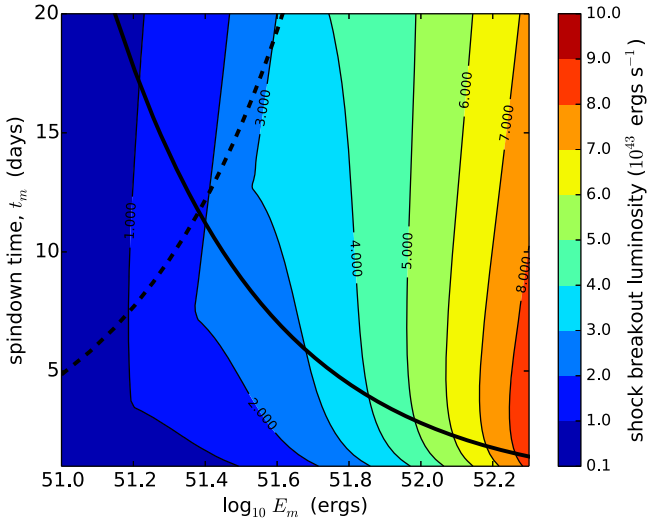

Figure 6. Same as Figure 3, but showing the calculated luminosity at the time of shock breakout.

deposition is spread out over a longer timescale, with $L_{\rm m}$ always less than $E_{\rm m}/t_{\rm m}$.

Figure 5 shows the time dependence of the local shock heating rate (Equation (20)) for continuous magnetar energy injection. The luminosity of the shock breakout pulse will approximately equal the local heating rate at the time of breakout. The local heating falls off with time roughly like a power law, owing to the progressive decrease in the preshock density. A break in the local heating rate is seen when the shock enters the steep density profile of the outer layers ($v > v_{\rm t}$). The shock is weakened at times $t > t_{\rm m}$ by the decrease in magnetar energy injection, and further at times $t \gtrsim t_{\rm d}$ by radiation diffusion through the ejecta shell, which depressurizes the magnetar bubble. The latter effect is included in the calculation by including a nonzero diffusion term $L_{\rm sn}$ in Equation (12).

3. OBSERVATIONAL CONSEQUENCES

3.1. Properties of Shock Breakout

To estimate the peak luminosity resulting from shock heating, we can use "Arnett's law" (Arnett 1982), which states that, for any general heating source, the luminosity at the light-curve peak is equal to the instantaneous rate of energy deposition at that time. We thus determine the peak luminosity by evaluating the heating rate Equation (20) at the shock breakout time, $t_{\rm bo}$,

$$L_{\rm bo} = 2\pi\zeta_\rho \frac{M_{\rm sn} v_{\rm t}^2}{t_{\rm bo}} \eta^3 \left(\frac{v_{\rm bo}}{v_{\rm t}}\right)^{-n+5}. \quad (22)$$

Shock breakout occurs at a velocity coordinate $v_{\rm bo} = r_{\rm bo}/t_{\rm bo}$ determined from Equations (10) and (16),

$$v_{\rm bo} \approx 1.1 v_{\rm t} \left[\frac{t_{\rm d}}{t_{\rm m}}\frac{E_{\rm m}}{E_{\rm sn}}\right]^{\frac{2(1-\beta)}{n-2}}. \quad (23)$$

Evaluating Equation (22) at the velocity coordinate $v_{\rm bo}$ then gives the peak luminosity

$$L_{\rm bo} \approx 9\frac{E_{\rm sn}}{t_{\rm d}}\eta^3 \left[\frac{t_{\rm m}}{t_{\rm d}}\frac{E_{\rm sn}}{E_{\rm m}}\right]^{\frac{(n-8)(1-\beta)}{(n-2)}}. \quad (24)$$

For standard parameters ($\beta = 1/2$, $n = 10$) the exponent of the term in brackets is only $1/8$, and we see that the peak luminosity depends most sensitively on the shock strength parameter, η. The luminosity also depends on $E_{\rm sn}$, as this sets the ejecta expansion velocity and hence the size of the remnant at the time of breakout.

The spectrum of the breakout emission can be approximated by a quasi-blackbody with an effective temperature, $T_{\rm eff}$, determined by $L_{\rm bo} = 4\pi r_{\rm p}^2 \sigma T_{\rm eff}^4$, where $r_{\rm p}$ is the photospheric radius defined by the $\tau = 1$ surface. From Equation (8)

$$r_{\rm p} \approx 1.2 v_{\rm t} t_{\rm d} (t_{\rm bo}/t_{\rm d})^{(n-3)/(n-1)}. \quad (25)$$

Plugging fiducial parameters ($n = 10$, $\delta = 1$, $\beta = 1/2$) into Equations (16), (24), and (25), we arrive at analytic estimates of the time, luminosity, photospheric radius, and effective temperature at the time of a magnetar-driven shock breakout,

$$t_{\rm bo} \approx 10.8\, M_{\rm sn,5}^{3/8} E_{\rm sn,51}^{1/4} E_{\rm m,51}^{-1/2} t_{\rm m,5}^{1/2} \text{ days} \quad (26)$$

$$L_{\rm sh} \approx 2.1 \times 10^{43}\, \eta_{0.2}^3 M_{\rm sn,5}^{-1/2} E_{\rm sn,51}^{3/4} E_{\rm m,51}^{-1/8} t_{\rm m,5}^{1/8} \text{ erg s}^{-1} \quad (27)$$

$$r_{\rm p} \approx 7.6 \times 10^{14} M_{\rm sn,5}^{-0.04} E_{\rm sn,51}^{0.64} E_{\rm m,51}^{-0.39} t_{\rm m,5}^{0.39} \kappa_{0.1}^{0.11} \text{ cm} \quad (28)$$

$$T_{\rm eff} \approx 15,500\, \eta_{0.2}^{0.75} M_{\rm sn,5}^{-0.1} E_{\rm sn,51}^{-0.13} E_{\rm m,51}^{0.16} t_{\rm m,5}^{-0.16} \kappa_{0.1}^{-0.06} \text{ K}, \quad (29)$$

where $E_{\rm sn,51} = E_{\rm m}/10^{51}$ erg, $t_{\rm m,5} = t_{\rm m}/5$ days, and $\eta_{0.2} = \eta/0.2$. In most stellar shock breakout events, the duration of the burst is set by the light-crossing time of the ejecta; however, in the present case the ejecta is extended and the timescale is set by the diffusion time, $t_{\rm bo}$ (see, e.g., Chevalier & Irwin 2011; Piro 2013).

The analytic results are only approximate; as an improved estimate of the peak luminosity, we used our numerical integration of the shell evolution to evaluate the heating rate at the time of shock emergence. Figure 6 shows the numerical results in the $E_{\rm m}$–$t_{\rm m}$ parameter space. The luminosity increases

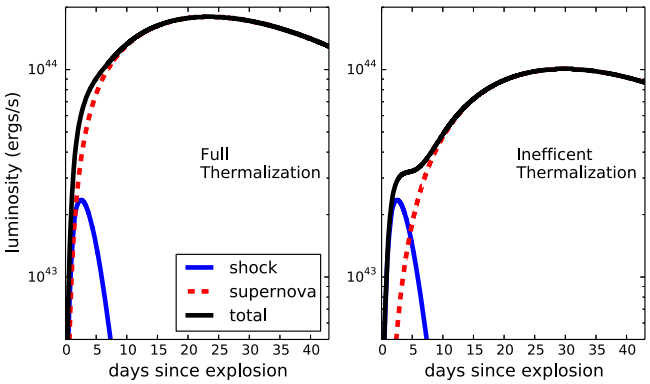

Figure 7. Approximate model light curves including both shock breakout emission (blue solid lines) and diffusive luminosity from magnetar heating (red dashed lines). The magnetar parameters are $E_{\rm m} = 5 \times 10^{51}$ erg and $t_{\rm m} = 2$ days, corresponding to $B_{14} = 4$, $P = 2.5$ ms. The SN ejecta had kinetic energy $E_{\rm sn} = 1 \times 10^{51}$ erg, mass 5 $M_\odot$, and opacity $\kappa = 0.1$ cm^2 g^{-1}. The right panel assumes 100% thermalization of magnetar energy; the left panel assumes inefficient thermalization according to Equation (33) with $Y = 0.1$, $A = 0.9$.

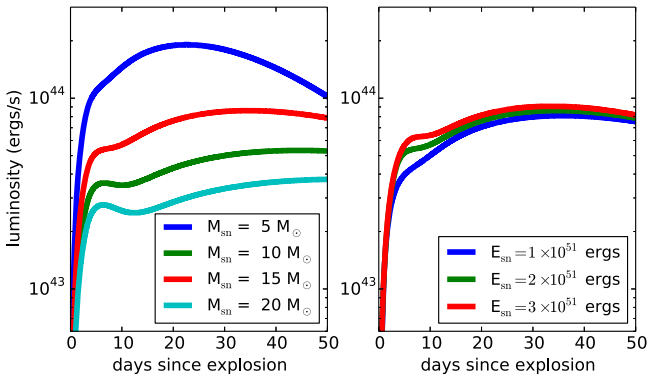

Figure 8. Approximate model light curves including both shock breakout emission and diffusive luminosity from magnetar heating. The magnetar parameters are $E_{\rm m} = 5 \times 10^{51}$ erg and $t_{\rm m} = 2$ days, corresponding to $B_{14} = 4$, $P = 2.5$ ms. In the left panel, the SN kinetic energy is $E_{\rm sn} = 10^{51}$ erg and the mass is in the range $M_{\rm sn} = 5$–$20\ M_\odot$. In the right panel, the SN mass is $M_{\rm sn} = 10\ M_\odot$ and the kinetic energy is in the range $E_{\rm sn} = (1$–$3) \times 10^{51}$ erg. The calculations assume 100% efficient magnetar thermalization and opacity $\kappa = 0.1$ cm^2 g^{-1}.

with $E_{\rm m}$ as higher magnetar energy drives a stronger shock (greater η). For low values of $t_{\rm m}$, the luminosity drops owing to the decline of η following magnetar shutoff.

3.2. Approximate Light Curves

The light curve of a magnetar-powered SN will be the sum of the emission from shock breakout and the diffusive luminosity from central magnetar heating. A first peak will only be distinguishable when the shock breakout luminosity is comparable to or greater than the diffusive luminosity at that time. To model the composite light curve, we used a one-zone formalism (Arnett 1982) to calculate approximate emission from each mechanism and then added the results. The method is described in the Appendix.

The left panel of Figure 7 shows a composite model bolometric light curve. For reasonable magnetar and ejecta parameters ($E_{\rm m} = 5 \times 10^{51}$ erg, $t_{\rm m} = 2$ days, $M_{\rm sn} = 5\ M_\odot$, $E_{\rm sn} = 10^{51}$ erg), the shock breakout emission is not dominant and produces only a kink in the early light-curve rise. The lack of a prominent first peak is consistent with the gray radiation-hydrodynamical calculations of Kasen & Bildsten (2010). Despite the lack of a distinct light-curve bump, the breakout may still be detectable by the shift in brightness and colors at the time of breakout, or by a sudden but small ($\sim$1000 km s^{-1}) increase in the line velocities when the photosphere recedes through the region of nonmonotonic velocity.

To see a clear double-peaked light curve requires either a very bright shock breakout or a slowly evolving diffusive light curve, properties that are only realized in certain regions of parameter space. Figure 8 shows that increasing the ejecta mass delays the diffusive light curve, making the shock breakout peak more prominent. Increasing the kinetic energy of the SN explosion leads to a larger remnant and brighter shock emission, which also clarifies the double-peaked structure. In addition, for very low SN and magnetar energies, $E_{\rm sn} \approx E_{\rm m} \approx 10^{50}$ erg, the main light curve evolves slowly and a low-luminosity double-peaked light curve can be seen.

Three additional physical effects may further distinguish the shock breakout peak: (1) Though the model light curves here and in Kasen & Bildsten (2010) assume a constant gray opacity, the true ejecta opacity likely increases inward, given the higher temperature and ionization state of the inner regions and the possible presence of synthesized iron group elements. A higher opacity in the interior would delay the diffusive light curve relative to the shock breakout emission. (2) Deviations from spherical symmetry due to bipolar magnetar energy injection may lead to breakout occurring first along the poles, making the breakout emission more conspicuous from polar viewing angles. (3) Inefficient thermalization of the magnetar wind would delay the rise of the diffusive light curve; we discuss this point in more detail in the next section.

4. MAGNETAR WIND THERMALIZATION

If the magnetar wind does not thermalize efficiently at early times, the rise of the diffusive light curve will be delayed, which will clarify the shock breakout peak. There are physical reasons to think that this delay in thermalization may occur in SLSNe.

The spindown luminosity of a magnetar is initially carried outward by a Poynting flux. The magnetic field is initially strong close to magnetar surface, becoming dominated by its toroidal component outside of the light cylinder radius. Eventually, reconnection inside the nebula (e.g., Porth et al. 2013; Mösta et al. 2014; Bromberg & Tchekhovskoy 2016) will convert the magnetic energy to high-energy $e^\pm$ particles. However, prior to the (uncertain) timescale for reconnection, the magnetar wind energy is not inefficiently thermalized and takes the form of a magnetically dominated outflow that drives a shock through the ejecta.

Even after reconnection dissipates the magnetic field energy, other physical effects may reduce the thermalization efficiency for a continued period of time. The dissipation of the wind energy at the termination shock or reconnection layers generates primarily high-energy $e^\pm$ pairs. The injected pairs cool rapidly via synchrotron and inverse Compton radiation, producing high-energy ($\gg m_e c^2$) photons that may in turn generate additional $e^\pm$ pairs by interacting with background thermal radiation (Metzger et al. 2014). The optical depth to γ–γ interactions is quantified by the

compactness parameter,

$$\ell \equiv \frac{E_{\rm nth}\sigma_{\rm T} r_{\rm n}}{V_{\rm n} m_e c^2} \approx 2000 L_{\rm m,45} t_{\rm day}^{-2} v_9^{-2}, \quad (30)$$

where $L_{,\rm m,45} = L_{\rm m}/10^{45}\ {\rm erg\ s^{-1}}$, $v_9 = v_{\rm t}/10^9\ {\rm cm\ s^{-1}}$, $t_{\rm day} = t/1\ {\rm day}$, $\sigma_{\rm T}$ is the Thomson cross section, $E_{\rm nth} \sim L_{\rm m} t$ is the approximate nonthermal energy injected into the nebula by the magnetar on the expansion time, $V_{\rm n} \approx 4\pi r_{\rm n}^3/3$ is the volume of the nebula, and $r_{\rm n} \sim v_{\rm t} t$ is the approximate nebula radius.

If $\ell \gg 1$, then pairs produced by the first generation of photons upscatter additional seed photons to sufficient energies to create additional pairs. The details of this "pair cascade" are complex, but the net effect is to convert a sizable fraction Y of the injected spindown power into $e^{\pm}$ pairs (e.g., Svensson 1987). The total number of pairs $N_{\pm}$ in the nebula is set by the equilibrium between the rate of pair creation and annihilation

$$\dot{N}_{\pm}^{+} \simeq \frac{Y L_{\rm m}}{m_e c^2} \quad \text{and} \quad \dot{N}_{\pm}^{-} = \frac{3}{16}\sigma_{\rm T} c N_{\pm}^2 V_{\rm n}^{-1}. \quad (31)$$

In equilibrium ($\dot{N}_{\pm}^{+} = \dot{N}_{\pm}^{-}$), the Thomson optical depth of pairs across the nebula is

$$\tau_{\rm es}^{\rm n} = \sigma_{\rm T} r_{\rm n} n_{\pm} = \left[\frac{4 Y \sigma_{\rm T} L_{\rm m}}{\pi r_{\rm n} m_e c^3}\right]^{1/2} \approx 19 Y^{1/2} L_{\rm m,45}^{1/2} v_9^{-1/2} t_{\rm day}^{-1/2}. \quad (32)$$

This equilibrium is reached on a timescale $t_{\rm eq} \simeq 16 r_{\rm n}/3c\tau_{\rm es}^{\rm n}$, which is short compared to the evolution timescale as long as $\tau_{\rm es}^{\rm n} \gg 16 v_{\rm t}/3c$.

Most of the remaining fraction $1 - Y$ of the energy released by the cooling $e^{\pm}$ pairs goes into a nonthermal power-law tail of radiation. The high scattering optical depth $\tau_{\rm es}^{\rm n}$ of the nebula traps these photons and delays their thermalization. On average, a hard photon must interact with the nebula walls $\sim(1 - A)^{-1}$ times before thermalizing, where the albedo A is the probability that the photon is scattered back into the nebula instead of being absorbed by the walls. The "lifetime" of a hard photon is therefore $t_{\rm life} = t_{\rm d}^{\rm n}(1 - A)^{-1}$, where $t_{\rm d}^{\rm n} \simeq (\tau_{\rm es}^{\rm n} + 1) r_{\rm n}/c$ is the photon diffusion time required for a single nebula crossing.

If $t_{\rm life}$ exceeds the expansion time, then nonthermal photons lose energy to adiabatic expansion before their energy can be thermalized. This reduces the effective rate of thermal energy production to a fraction of the magnetar spindown power (Metzger & Piro 2014)

$$L_{\rm th} = \frac{L_{\rm m}}{1 + (t_{\rm life}/t)}, \quad (33)$$

where

$$\frac{t_{\rm life}}{t} = \frac{\tau_{\rm es}^{\rm n} v_{\rm t}}{c(1 - A)} \approx 0.6 \frac{Y^{1/2}}{1 - A} L_{\rm m,45}^{1/2} v_9^{1/2} t_{\rm day}^{-1/2} \quad (34)$$

and we have assumed $\tau_{\rm es}^{\rm n} \gg 1$.

Depending on the characteristic values of Y and A, suppression of the magnetar power due to thermalization can be important. A typical value of the pair multiplicity is $Y \sim 0.1$ (Svensson 1987), although its precise value will depend on the nature of the pair cascade and deserves further study. The albedo depends on the ionization parameter, which sets the ratio of scattering to absorption in the ejecta wall. Photoionization calculations by Ross et al. (1999) (their Figure 2) show a rather high albedo $A \sim 0.9$ across a range of photon energies ~1–30 keV, although for high photon energies inelastic scattering results in a higher absorbed fraction.[6]

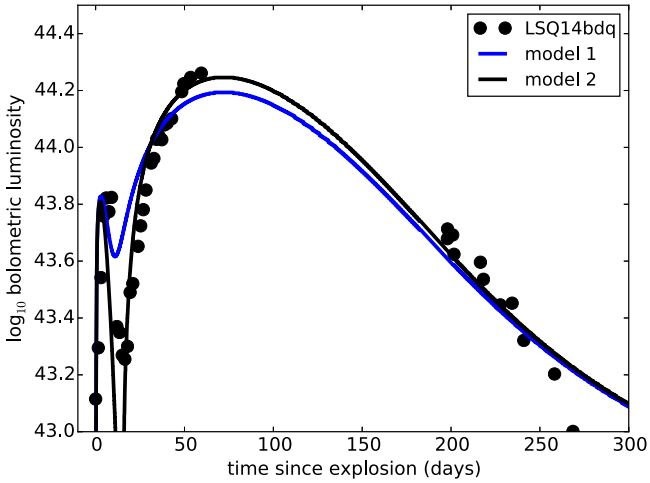

Figure 9. Comparison of the observed bolometric light curve of SN-LSQ14BDQ (black circles) with model light curves with parameters $M_{\rm sn} = 25\,M_{\odot}$, $E_{\rm sn} = 5 \times 10^{51}$ erg, $t_{\rm m} = 1.5$ days, and $E_{\rm m} = 5 \times 10^{52}$ erg. Model 1 (blue lines) assumes that the magnetar wind energy is inefficiently thermalized as described by Equation (33). Model 2 (black lines) simply assumes that the thermalization is completely inefficient for $t < 15$ days, and 100% efficient thereafter. The latter approach provides more contrast in the peaks.

For values $Y = 0.1$, $A = 0.9$, thermalization of the magnetar wind will be suppressed for ~1 week following the explosion. Inefficient thermalization will not affect the dynamics of the shock, but will reduce the early diffusive luminosity from direct magnetar heating. We included this effect in our light-curve calculations by using the suppressed magnetar luminosity Equation (33) to determine the SN light curve. The results, shown in the right panel of Figure 7, demonstrate that inefficient thermalization may serve to better distinguish the double-peaked light-curve shape.

5. DISCUSSION AND CONCLUSIONS

The predicted luminosity and timescale of magnetar-driven shock breakout are compellingly similar to those seen in the double-peaked light curves of some SLSNe. As a concrete example, Figure 9 compares approximate light-curve models with the observed bolometric light curve of SN-LSQ14BDQ (as constructed by Nicholl et al. 2015). The models have $M_{\rm sn} = 25\,M_{\odot}$, $E_{\rm sn} = 5 \times 10^{51}$ erg, $t_{\rm m} = 1.5$ days, and $E_{\rm m} = 5 \times 10^{52}$ erg, although we do not claim these values to be optimal or unique. The adopted magnetar energy is high, but well within the possible range recently found for rapidly rotating neutron stars (Metzger et al. 2015).

To see a clear double peak in the models of Figure 9 required that we assumed inefficient magnetar heating at early times. We tried two ways of implementing this: the first used the

[6] Also note that we have assumed that photons absorbed by the ejecta are immediately thermalized. However, in reality if their energy is instead deposited in the electrons in the hot outer ionized layer (where the Compton temperature is much higher), additional Compton downscattering may be required to diffuse this energy to optical/UV wavelengths, resulting in an effective value of A that is even higher.

suppression function Equation (33); the second simply assumed that heating was completely inefficient until a time $t = 15$ days, and 100% efficient thereafter. The latter results in a clearer separation of the two light-curve peaks, in better agreement with the observations. Clearly, the uncertain details of magnetar wind thermalization are important in setting the precise shape of the early-time light curve. The failure of the model to fit the observations at $t > 250$ days may also be due to a decrease in thermalization efficiency at late times (for distinct physical reasons).

The reasonable model fits shown in Figure 9 suggest that the breakout scenario holds some promise for explaining double-peaked SLSNe. However, one should not put too much weight on this comparison (or the inferred physical parameters) given the number of approximations that have gone into our model light curves. In particular, we have made coarse assumptions regarding spherical symmetry, the efficiency of thermalization, and the treatment of the radiative transfer. Detailed radiation-hydrodynamical calculations are needed to make more meaningful comparisons to data.

If, in contrast to the models of Figure 9, thermalization is efficient at early times, the shock breakout peak is typically not easily distinguished from the diffusive luminosity from central magnetar heating. To explain a double-peaked light curve in this case requires a specific set of parameters—an SN with a large ejecta mass ($M_{\rm sn} \gtrsim 15\,M_\odot$) and/or a high explosion energy ($E_{\rm sn} \gtrsim 3 \times 10^{51}$ erg). For high ejecta masses, one might expect the collapsing stellar core to form a black hole rather than a neutron star. Most of our discussion of driven shock emission applies equally to an engine powered by black hole accretion (Dexter & Kasen 2013), in which case the energy input is set by the rate of fallback.

Deviations from our assumption of spherical symmetry presumably affect the luminosity and timescale of breakout. The actual geometry is likely bipolar, as even a sub-equipartition toroidal magnetic field can act through hoop stress to confine the nebular pressure along the rotational axis. The resulting anisotropic stress may drive a weak, wide-angle "jet" (Bucciantini et al. 2007), and the shocked ejecta will take the form of a broad "cocoon" that enshrouds that jet (as has been discussed for normal gamma-ray bursts [GRBs]; e.g., Lazzati & Begelman 2005). In SLSNe, the shock breakout of this "cocoon" would emerge continuously over a timescale of several days or longer, as set by the engine duration and the large size of the remnant. Our spherical analysis here may still be used to roughly estimate the dynamics, but with the input magnetar power enhanced by a factor of $4\pi/\Omega$, where Ω is the solid angle of the "jet."

Jet-like collimation of the energy should presumably result in a brighter shock breakout, at least for some viewing angles. This may make double-peaked light curves conspicuous even when inefficient magnetar heating is not invoked. The light curve will depend on orientation, with the breakout emission being more prominent for polar viewing angles and less so for equatorial views. Because the jet cocoon is expected to be fairly broad, bipolar, and nonrelativistic, at least some breakout emission is likely to be emitted in all directions.

We have not considered how energy is thermalized behind the magnetar-driven shock. Katz et al. (2010) show that, in SN shock breakout, the postshock gas and radiation reach equilibrium for shock velocities $v/c \lesssim 0.1$. The velocities expected here are much lower, $v_{\rm s} - v_{\rm ej} \approx 0.01c$. Once the shock emerges, however, and if it continues to be driven into low-density, optically thin ejecta, equilibrium may no longer be reached. In this case, one could look for some fraction of the shock heating emerging as nonthermal X-ray or radio emission. Figure 5 shows that, for typical parameters, the shock heating rates are $\sim 10^{43}$–10^{44} erg s^{-1} at day 10, dropping to 10^{41}–10^{42} erg s^{-1} by days 50–100.

The dynamical effect of magnetar energy injection has additional observational consequences. An abrupt but small increase in the Doppler shifts of line absorption features (by an amount $\approx$1000 km s^{-1}) may occur when the photosphere recedes into the region of nonmonotonic ejecta velocities created by the shock (see Figure 1). Following this, the photospheric velocity should coincide with the motion of the swept-up shell. For long spindown times, the shell may still be accelerating at the time at which spectra are taken, such that the photospheric velocity *increases* with time, counter to the behavior expected for free expansion. Such an effect may have been observed in the helium lines of SN 2005bf (Tominaga et al. 2005), a double-peaked SN Ib that Maeda et al. (2007) modeled with magnetar heating. Once the magnetar has shut off, the shell and photospheric velocity should approach a constant value over time. These expectations may have to be modified to account for asymmetries due to an anisotropic magnetar wind or hydrodynamical instabilities in the shell.

The magnetar model is but one explanation of double-peaked SLSN light curves. While the first peak in SN-LSQ14BDQ was too brief and bright to be explained by ^{56}Ni heating, possible alternative mechanisms include cooling emission from a hyperenergetic SN explosion (Nicholl et al. 2015) or interaction with a dense CSM (Moriya & Maeda 2012; Piro 2015). In either case the necessary ejecta kinetic energy is large, (4–50) $\times$ 10^{51} erg, depending on the assumed radius of the star or CSM shell (Nicholl et al. 2015; Piro 2015). The second light-curve peak requires a distinct mechanism, either central engine heating or interaction with an additional CSM shell at larger radius. While such a multi-component scenario cannot be ruled out, it is appealing that the magnetar model alone may be able to reproduce the double peak without introducing additional model parameters, or requiring extreme values of the existing ones.

Determining the fraction of SLSNe with double-peaked light curves would help discriminate the mechanism responsible. Models that explain both peaks with CSM interaction require two distinct CSM shells—one low-mass, nearby shell and one higher-mass, more distant shell. There is no obvious reason why pre-SN mass loss would conspire to frequently produce such a configuration. In the magnetar model, on the other hand, some early time emission from shock breakout is a generic consequence of the central energy injection.

Spectra taken at the time of the first peak would also be diagnostic. Magnetar-driven shock breakout is expected to produce a blue ($T_{\rm eff} \approx$ 20,000 K) quasi-blackbody spectrum that is mostly featureless owing to the high temperature and ionization state. Any detectable line features would be of high velocity ($\gtrsim$ 10,000 km s^{-1}). In the CSM interaction models, in contrast, one might expect narrow line emission from a photoionized, slowly moving CSM shell, or perhaps narrow line absorption if a second, cold CSM shell exists at larger radius.

While the magnetar model has been most frequently invoked to explain SLSNe, a lower level of magnetar powering may

occur in less luminous SNe, perhaps in some cases producing a double-peaked light curve. For example, for SNe where the explosion energy and magnetar energy are both $\approx 10^{50}$ erg, the predicted shock breakout luminosity is only $\approx 10^{42}$ erg s^{-1}, but produces a noticeable early peak in the light curve.

If double-peaked SLSN light curves are indeed due to shock breakout, this may indicate an interesting connection with the recently discovered class of very long duration GRBs. Greiner et al. (2015) present observations of a $\sim 10^4$ s long GRB that had an associated superluminous optical transient, both of which they argue are powered by a magnetar. Metzger et al. (2015) suggested that the jet in this event was just barely powerful enough to escape the stellar remnant. For events with longer magnetar spindown timescales $\gtrsim 10^4$ s, or higher ejecta masses, a relativistic GRB jet may fail to emerge; however, the underlying engine may still be revealed by the breakout of the magnetar-driven shock (or "cocoon") producing a double-peaked optical light curve.

While the calculations in this paper have outlined the main features of magnetar-driven shock breakout, radiation-hydrodynamical calculations that include realistic opacities and, ideally, magnetic fields and departures from spherical symmetry are needed for detailed predictions. The observational constraints on the magnetar model are now many: the timescale and luminosity of the first peak, the shape and brightness of the second peak, the photospheric velocity evolution, and the luminosity, color, and decline rate of the late-time tail emission. Simultaneous fitting of all of these observables within the limited model parameters (B, P, $M_{\rm sn}$, $E_{\rm sn}$) constitutes a non-trivial test of the paradigm.

We thank Roger Chevalier, Tony Piro, Eliot Quataert, Stephen Smartt, Tuguldor Sukhbold, and Stan Woosley for helpful conversations and comments on the draft, and Matt Nicholl for providing the bolometric light-curve data for SN-LSQ14BDQ. D.K. is supported in part by a Department of Energy Office of Nuclear Physics Early Career Award, and by the Director, Office of Energy Research, Office of High Energy and Nuclear Physics, Divisions of Nuclear Physics, of the U.S. Department of Energy under Contract No. DE-AC02-05CH11231. B.D.M. gratefully acknowledges support from the NSF grant AST-1410950 and the Alfred P. Sloan Foundation. This work was supported by the National Science Foundation under grants PHY 11-25915, AST 11-09174, and AST 12-05574. This work was supported in part by NSF Grant No. PHYS-1066293 and the hospitality of the Aspen Center for Physics.

APPENDIX

To calculate approximate light curves, we use a one-zone formalism (Arnett 1982) that has frequently been applied to model magnetar-powered light curves (e.g., Kasen & Bildsten 2010; Inserra et al. 2013). To model the SN light curve powered by direct magnetar heating, we consider the evolution of the internal energy, $E_{\rm int}$, of the bulk of the ejecta

$$\frac{dE_{\rm int}}{dt} = -p\frac{dV}{dt} + L_{\rm m} - L_{\rm sn}, \tag{35}$$

where V is the volume and p is the pressure. In the diffusion approximation, the radiated luminosity is

$$L_{\rm sn} = 4\pi R^2 \frac{c}{3\kappa\rho}\frac{\partial (E_{\rm int}/V)}{\partial R} \approx \frac{4\pi c R^2}{3\kappa\rho}\frac{(E_{\rm int}/V)}{R}. \tag{36}$$

Assuming homologous expansion ($R = vt$) gives

$$L_{\rm sn} \approx E_{\rm int} t/t_{\rm sn}^2 \ \text{ where } t_{\rm sn} = \left[\frac{3\kappa M_{\rm sn}}{4\pi v c}\right]^{1/2}. \tag{37}$$

The timescale $t_{\rm sn}$ is similar to the diffusion time $t_{\rm d}$ (Equation (9)), although here we include the energy input by the magnetar to calculate the velocity, $v = [2(E_{\rm sn} + E_{\rm m})/M_{\rm sn}]^{1/2}$.

The formal solution to the differential Equation (35) is

$$L_{\rm sn} = e^{-(t/t_{\rm sn})^2}\int_0^t 2L_{\rm m}(t'/t_{\rm sn})e^{-(t'/t_{\rm sn})^2}dt'. \tag{38}$$

The treatment here is clearly approximate, as it neglects the formation and expansion of the shell structure. Previous calculations have shown, however, that the one-zone formalism well reproduces the light curves from more detailed radiation-hydrodynamical models (Inserra et al. 2013).

To calculate the luminosity due to magnetar-driven shock heating, we solve an independent one-zone model, using the same integral expression given by Equation (38) but with the heating rate $L_{\rm m}$ replaced with the shock heating rate $\dot{\epsilon}_{\rm sh}$ (from Equation (20)). The time-dependent $\dot{\epsilon}_{\rm sh}$ was determined from our numerical integration of the shell dynamics (see Figure 5). We further replace $t_{\rm sn}$ with $t_{\rm bo}$ (Equation (16)), as $t_{\rm bo}$ gives the appropriate timescale when the diffusion time from the shock-heated region equals the elapsed time. In these calculations we use Equation (38) to include the radiative loss term in the shell evolution, i.e., $L_{\rm sn} \neq 0$ in the energy equation (Equation (12)). The two one-zone model light curves were summed to give the composite SN light curve.

REFERENCES

Anupama, G. C., Sahu, D. K., Deng, J., et al. 2005, ApJL, 631, L125
Arnett, W. D. 1982, ApJ, 253, 785
Barbary, K., Dawson, K. S., Tokita, K., et al. 2009, ApJ, 690, 1358
Blondin, J. M., Chevalier, R. A., & Frierson, D. M. 2001, ApJ, 563, 806
Bodenheimer, P., & Ostriker, J. P. 1974, ApJ, 191, 465
Bromberg, O., & Tchekhovskoy, A. 2016, MNRAS, 456, 1739
Bucciantini, N., Quataert, E., Arons, J., Metzger, B. D., & Thompson, T. A. 2007, MNRAS, 380, 1541
Chevalier, R. A. 1984, ApJ, 280, 797
Chevalier, R. A. 2005, ApJ, 619, 839
Chevalier, R. A., & Fransson, C. 1992, ApJ, 395, 540
Chevalier, R. A., & Irwin, C. M. 2011, ApJL, 729, L6
Chevalier, R. A., & Soker, N. 1989, ApJ, 341, 867
Chomiuk, L., Chornock, R., Soderberg, A. M., et al. 2011, ApJ, 743, 114
Dessart, L., Hillier, D. J., Waldman, R., Livne, E., & Blondin, S. 2012, MNRAS, 426, L76
Dexter, J., & Kasen, D. 2013, ApJ, 772, 30
Folatelli, G., Contreras, C., Phillips, M. M., et al. 2006, ApJ, 641, 1039
Gaffet, B. 1977, ApJ, 216, 852
Gal-Yam, A. 2012, Sci, 337, 927
Greiner, J., Mazzali, P. A., Kann, D. A., et al. 2015, Natur, 523, 189
Howell, D. A., Kasen, D., Lidman, C., et al. 2013, ApJ, 779, 98
Inserra, C., Smartt, S. J., Jerkstrand, A., et al. 2013, ApJ, 770, 128
Kasen, D., & Bildsten, L. 2010, ApJ, 717, 245
Katz, B., Budnik, R., & Waxman, E. 2010, ApJ, 716, 781
Klein, R. I., & Chevalier, R. A. 1978, ApJL, 223, L109
Lazzati, D., & Begelman, M. C. 2005, ApJ, 629, 903
Leloudas, G., Chatzopoulos, E., Dilday, B., et al. 2012, A&A, 541, A129
Maeda, K., Tanaka, M., Nomoto, K., et al. 2007, ApJ, 666, 1069

Matzner, C. D., & McKee, C. F. 1999, ApJ, 510, 379
Metzger, B. D., Margalit, B., Kasen, D., & Quataert, E. 2015, MNRAS, 454, 3311
Metzger, B. D., & Piro, A. L. 2014, MNRAS, 439, 3916
Metzger, B. D., Vurm, I., Hascoët, R., & Beloborodov, A. M. 2014, MNRAS, 437, 703
Moriya, T., Tominaga, N., Blinnikov, S. I., Baklanov, P. V., & Sorokina, E. I. 2011, MNRAS, 415, 199
Moriya, T. J., & Maeda, K. 2012, ApJL, 756, L22
Mösta, P., Richers, S., Ott, C. D., et al. 2014, ApJL, 785, L29
Nicholl, M., Smartt, S. J., Jerkstrand, A., et al. 2013, Natur, 502, 346
Nicholl, M., Smartt, S. J., Jerkstrand, A., et al. 2014, MNRAS, 444, 2096
Nicholl, M., Smartt, S. J., Jerkstrand, A., et al. 2015, ApJL, 807, 18
Ofek, E. O., Cameron, P. B., Kasliwal, M. M., et al. 2007, ApJL, 659, L13
Ostriker, J. P., & Gunn, J. E. 1971, ApJL, 164, L95
Papadopoulos, A., D'Andrea, C. B., Sullivan, M., et al. 2015, MNRAS, 449, 1215
Pastorello, A., Smartt, S. J., Botticella, M. T., et al. 2010, ApJL, 724, L16
Piro, A. L. 2013, ApJL, 768, L14
Piro, A. L. 2015, ApJL, 808, 51
Porth, O., Komissarov, S. S., & Keppens, R. 2013, MNRAS, 431, L48
Quimby, R. M., Aldering, G., Wheeler, J. C., et al. 2007, ApJL, 668, L99
Quimby, R. M., Kulkarni, S. R., Kasliwal, M. M., et al. 2011, Natur, 474, 487
Ross, R. R., Fabian, A. C., & Young, A. J. 1999, MNRAS, 306, 461
Smith, N., Li, W., Foley, R. J., et al. 2007, ApJ, 666, 1116
Smith, N., & McCray, R. 2007, ApJL, 671, L17
Svensson, R. 1987, MNRAS, 227, 403
Tominaga, N., Tanaka, M., Nomoto, K., et al. 2005, ApJL, 633, L97
Woosley, S. E. 2010, ApJL, 719, L204
Woosley, S. E., Blinnikov, S., & Heger, A. 2007, Natur, 450, 390